AIP | Applied Physics Letters

Electro-photo double modulation on the resistive switching behavior and switchable photoelectric effect in BiFeO3 films

Le Wang, Kui-juan Jin, Chen Ge, Can Wang, Hai-zhong Guo et al.

Citation: Appl. Phys. Lett. **102**, 252907 (2013); doi: 10.1063/1.4812825
View online: http://dx.doi.org/10.1063/1.4812825
View Table of Contents: http://apl.aip.org/resource/1/APPLAB/v102/i25
Published by the AIP Publishing LLC.

Electro-photo double modulation on the resistive switching behavior and switchable photoelectric effect in $BiFeO_3$ films

Le Wang, Kui-juan Jin,[a] Chen Ge, Can Wang, Hai-zhong Guo, Hui-bin Lu, and Guo-zhen Yang
Beijing National Laboratory for Condensed Matter Physics, Institute of Physics, Chinese Academy of Sciences, Beijing 100190, China

(Received 23 January 2013; accepted 9 June 2013; published online 28 June 2013)

We present an electro-photo double modulation on the resistive switching behavior in an Au/$BiFeO_3$/$La_{0.7}Sr_{0.3}MnO_3$/$SrTiO_3$ heterostructure, combining the electro-resistance effect and the photo-resistance effect. The pulse voltages can lead to nonvolatile resistance variations in this heterostructure, and the laser illumination can also modulate the high and low resistance states. Consequently, four stable resistance states are achieved. Furthermore, a switchable photoelectric effect-the direction of the photocurrent can be switched by polarization reversal, is also observed in this heterostructure. The present results should have potential applications to develop multi-state memory devices based on perovskite oxides. © *2013 AIP Publishing LLC*. [http://dx.doi.org/10.1063/1.4812825]

Ferroelectrics are characterized by a spontaneous polarization that occurs below the Curie temperature and can be switched between at least two different states of different electric polarizations by using an external electric field.[1] Two opposite polarization states represent two different resistance states, which can be used in the ferroelectric resistive random-access memory (FeRRAM) technology.[2,3] Compared with magnetic random access memories (MRAMs), important attributes of FeRRAMs are ultrafast operating speeds and the high resistance ratio.[4,5] Furthermore, a number of recent studies have been focused on photo-induced effects in ferroelectrics because of their tunable photovoltage output.[6–9] It is important to realize that photo-induced effect can be coupled with other functional properties of ferroelectrics.[10] Recently, we reported a pronounced electro-resistance effect[11,12] induced by the ferroelectric polarization and a photo-resistance effect[13] illuminated by an ultraviolet laser in $BiFeO_3$ (BFO) thin films. In this work, we present an electro-photo double modulation resistive switching behavior in the Au/$BiFeO_3$/$La_{0.7}Sr_{0.3}MnO_3$/$SrTiO_3$ (Au/BFO/LSMO/STO) heterostructure, combining the electro-resistance effect and the photo-resistance effect. A four-state electro-photo resistive modulation was observed in the Au/BFO/LSMO/STO heterostructure. It was found that the high and low resistance states of the Au/BFO/LSMO/STO heterostructures can be switched by applying the positive and negative pulse voltages, and the laser illumination can also modulate the resistance states. Furthermore, we have also observed the switchable photoelectric effect in this heterostructure, and proposed that the variations of Schottky barriers at the interfaces between the electrodes and BFO with ferroelectric polarization reversal play a key role in the switchable photoelectric effect. Based on the present results, it is promising that the multi-state resistive switching behavior would be realized by introducing photo-related parameter (such as the wavelength and the intensity, etc.) and structure optimization in the metal/ferroelectrics/metal sandwich system.

BFO/LSMO heterostructure was deposited on STO (001) single crystals by a laser molecular-beam epitaxy system (laser-MBE)[14] using a XeCl 308 nm excimer laser with an energy density of ~2 J/cm^2 and a repetition rate of 2 Hz. The BFO layer with the thickness of 300 nm and the LSMO layer of 120 nm were deposited at the oxygen pressures of 10 and 40 Pa, and the deposition rates of the BFO and LSMO layers were ~1.5 and 4 nm/min, respectively. The substrate temperature detected by an infrared pyrometer was kept about 580 °C. After deposition, the sample was annealed at the same temperature under the oxygen pressure of 3 kPa for 20 min, and then cooled down to room temperature. LSMO is used as a conducting bottom layer. Piezoresponse force microscopy (PFM, Asylum Research MFP-3D) images were collected and recorded using a Ti/Ir-coated Si cantilever (Olympus Electrilever) with a nominal ~2 N/m spring constant and a free air resonance frequency of ~70 kHz. Sample poling was performed in the lithography mode by applying a voltage of ±9.8 V to the tip during the scan. The scanning rates of writing bitmap and reading bitmap were 0.1 and 0.5 Hz, respectively. The voltage of the reading bitmap was 2 V. For the photovoltaic and ferroelectric measurements, circular Au top electrodes with a diameter of 100 μm and a thickness of 50 nm were sputtered on the BFO films using a metal shadow mask. The ferroelectric hysteresis loops of the Au/BFO/LSMO/STO heterostructure were measured using a Radiant Technologies RT6000 ferroelectric test system at 10 kHz. The photoelectric properties of the Au/BFO/LSMO/STO heterostructure were investigated under the illumination of a continuous blue laser (Oxxius, wavelength of 375 nm and power density of 0 ~ 840 mW/cm^2). The current-voltage (I-V) curves of the Au/BFO/LSMO/STO heterostructure were measured using a computer-controlled meter (Keithley 2400). The pulse voltage, we used to switch the polarization state of the BFO layers, was an asymmetric square wave with a delay time of 200 ms. Junction resistances (defined as V/I, where V is the measurement voltage and I is the current) of the Au/BFO/LSMO/STO heterostructure were measured with a high-resistance meter (Keithley 6517) in dark and

[a]Author to whom correspondence should be addressed. Electronic mail: kjjin@iphy.ac.cn

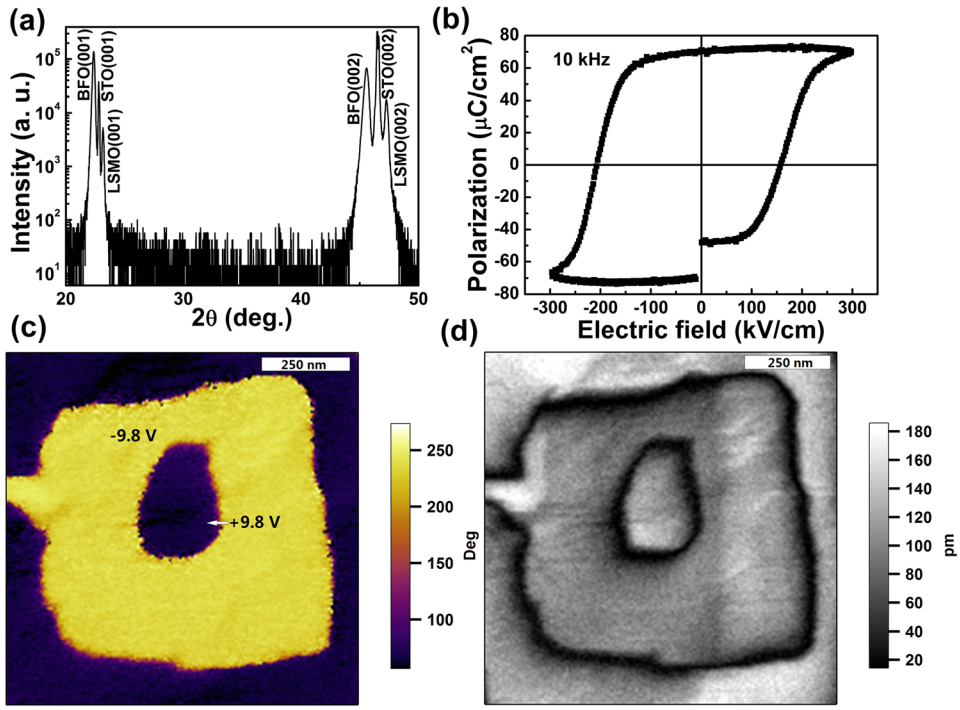

FIG. 1. (a) X-ray diffraction patterns for the BFO/LSMO/STO heterostructure at room temperature. (b) The *P-E* loop of the Au/BFO/LSMO/STO heterostructure at 300 K with 10 kHz frequency. (c) OP-PFM phase and (d) amplitude images of the BFO film after applying +9.8 V (inner square) and −9.8 V (outer square) bias at the center of the region.

under the illumination of the 375 nm laser through the top Au electrodes.

X-ray diffraction pattern of the BFO/LSMO/STO heterostructure shown in Fig. 1(a) indicates that both the LSMO and BFO layers are highly textured. Figure 1(b) shows the polarization-electric field (*P-E*) hysteresis loop of the Au/BFO/LSMO/STO heterostructure measured at 10 kHz. In this work, forward (reverse) bias is defined as a positive voltage applied on the bottom (top) electrode, and the polarization pointing from the bottom (top) electrode to the top (bottom) electrode is defined as the upward (downward) polarization. The *P-E* loop is saturated at a bias of 18 V_{pp} (600 kV/cm), where V_{pp} is the peak to peak voltage. A remanent polarization P_r of 72 $\mu C/cm^2$ indicates a well ferroelectric property of the BFO film. Figures 1(c) and 1(d) show the phase and amplitude images of the out-of-plane PFM (OP-PFM), respectively. The images show the two opposite polarization domains evidenced from the bright contrast of colors. The two opposite polarization states will provide a foundation for investigating the polarization-dependent resistance characteristics and photoelectric effect in the BFO layers.

To investigate the electro-photo double modulation on the resistive switching behavior, the time dependence of the junction resistances of the Au/BFO/LSMO/STO heterostructure in dark and under the illumination of a 375 nm laser (840 mW/cm^2) was measured, as shown in Fig. 2(a). The

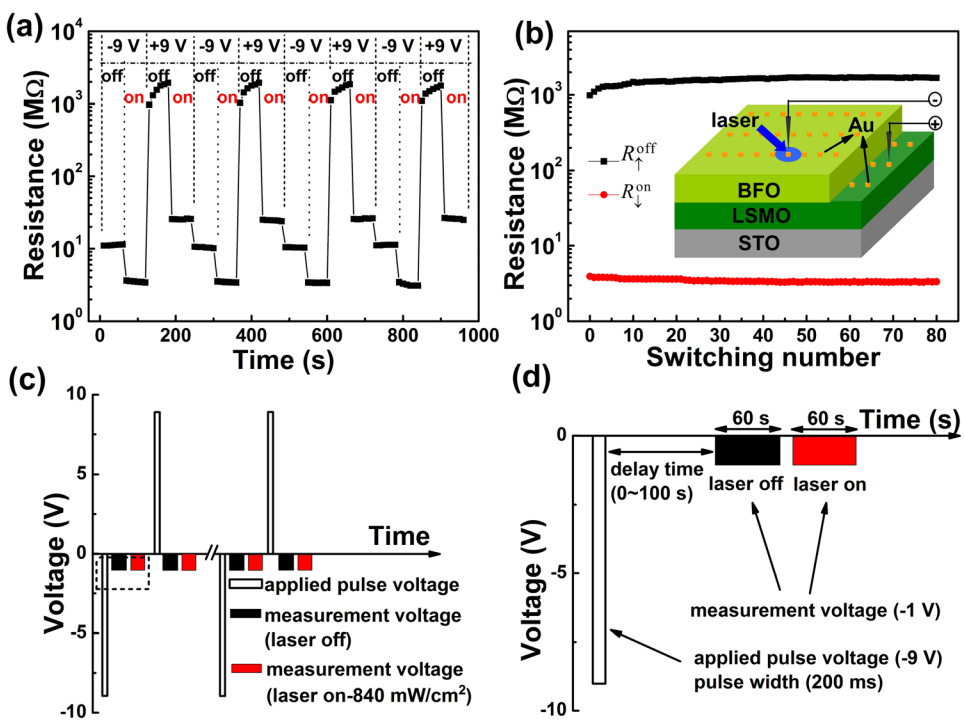

FIG. 2. (a) Variations in the junction resistances of the Au/BFO/LSMO/STO heterostructure with −9 V and +9 V pulse voltages measured at −1 V in dark and under the illumination of the 375 nm laser (840 mW/cm^2). (b) The high and low resistance states with repetition of polarization-orientation switching. The inset shows the measurement setup schematic. (c) The schematic of applied pulse voltage train and the measurement voltage vs. time. (d) The magnification of the area marked by short dashed rectangle in (c).

375 nm laser was fixed to a probe station and focused into an ellipsoidal spot with an area of $\sim 2.2 \times 1.3\,mm^2$. The incident angle was about 45°. The test structure was contacted by using a Tungsten probe with a diameter of 10 μm. The measurement setup schematic was shown in the inset of Fig. 2(b). The variations of the junction resistances with a train of −9 V (−300 kV/cm) and +9 V (+300 kV/cm) pulse voltage were measured at −1 V. It was observed that four stable resistance states $R_{\downarrow}^{off}$, $R_{\downarrow}^{on}$, $R_{\uparrow}^{off}$, and $R_{\uparrow}^{on}$ were achieved, with "on" and "off" indicating the two states of the 375 nm laser, and the arrow indicating the polarization direction. Here, we define the electro-photo modulated resistance (EPR) ratio as $\frac{(R_{\uparrow}^{off}-R_{\downarrow}^{on})\times 100\%}{R_{\downarrow}^{on}}$. It is interesting to note that the EPR ratio is about 46 000%, which is larger than both the electro-resistance ratio $\frac{(R_{\uparrow}^{off}-R_{\downarrow}^{off})\times 100\%}{R_{\downarrow}^{off}} = 16000\%$ and the photo-resistance ratio $\frac{(R_{\uparrow}^{off}-R_{\uparrow}^{on})\times 100\%}{R_{\uparrow}^{on}} = 7200\%$ ($\frac{(R_{\downarrow}^{off}-R_{\downarrow}^{on})\times 100\%}{R_{\downarrow}^{on}} = 240\%$) after upward (downward) polarization. To evaluate the stability of the heterostructures, we performed repeatable switching of the ferroelectric polarization for 80 times. No significant changes in the resistances were observed (as shown in Fig. 2(b)), indicating that the heterostructures are stable. The schematic of applied pulse voltage train and the measurement voltage vs. time is shown in Fig. 2(c). Figure 2(d) is the magnification of the area marked by a short dashed rectangle in Fig. 2(c). These results will open the perspective of combining multiple degrees of freedom in controlling the resistive switching behavior.

The *I-V* loops of the Au/BFO/LSMO/STO heterostructure at room temperature are shown in Fig. 3(a). The arrows in Fig. 3(a) denote the sequence of voltage sweeps. *I-V* curves in dark show distinct hysteresis behavior, indicating the electro-resistance effect. The currents under the illumination of the 375 nm laser obviously increase, especially at the negative voltages region, indicating the photo-resistance effect. Figure 3(b) shows the *I-V* curves of the Au/BFO/LSMO/STO heterostructure after upward and downward polarization in dark and under the illumination of the 375 nm laser. From Fig. 3(b), it can be seen that the *I-V* curve after upward or downward polarization in dark shows obvious diode-like rectifying characteristic, and the diode directions can be switched when the ferroelectric polarization is reversed by applying pulse voltages. Moreover, the switchable photoelectric effect is observed under the illumination of the 375 nm laser. The direction of the short-circuit current (I_{sc}) is always opposite to the diode's forward direction. I_{sc} after downward polarization is about +170 nA, larger than that after upward polarization. On the other hand, the open-circuit photovoltage (V_{oc}) after downward polarization is about −0.75 V, also larger than that after upward polarization. The photovoltaic efficiency of the Au/BFO/LSMO/STO heterostructure after downward polarization under the illumination of the 375 nm laser is about $5.5 \times 10^{-2}\%$, which is comparable to that of BFO/Nb-doped-$SrTiO_3$ ($3 \times 10^{-2}\%$)[15] and higher than that in the BFO (001) thin films ($1.2 \times 10^{-5}\%$).[16]

According to the work functions of the top and bottom electrode materials and the affinity of BFO,[17–19] the values

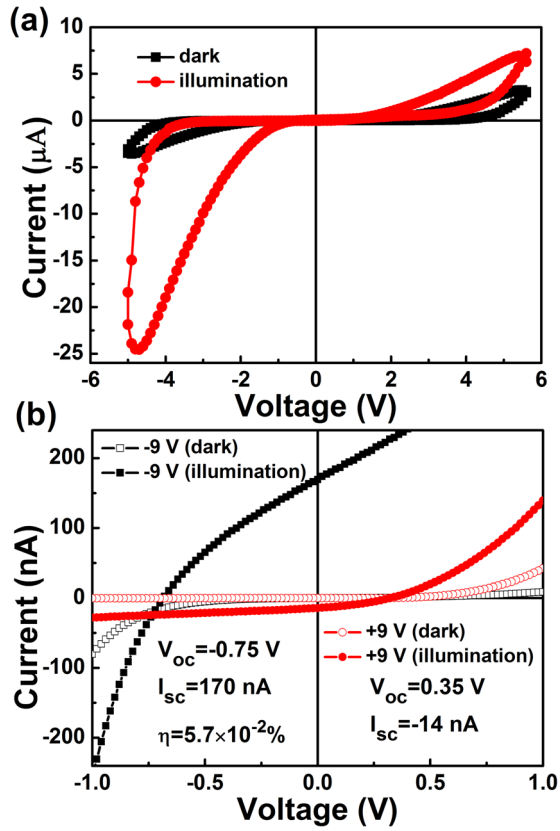

FIG. 3. (a) The *I-V* curves of the Au/BFO/LSMO/STO heterostructure at room temperature. The open symbols are for the *I-V* curves in dark, and the solid symbols indicate the *I-V* curves under the illumination of the 375 nm laser (840 mW/cm^2). (b) *I-V* curves for the Au/BFO/LSMO/STO heterostructure after upward polarization (+9 V) and downward polarization (−9 V) in dark and under the illumination of the 375 nm laser (840 mW/cm^2).

of the Schottky barrier height at the Au/BFO interface and the LSMO/BFO interface are estimated to be 1.8 and 1.5 eV, respectively. It is well known that the ferroelectric polarization plays a dominant role in the transport of the metal/ferroelectrics/metal structures.[12,20,21] For the Au/BFO/LSMO/STO heterostructure after upward polarization, due to the negative polarization charges, the built-in field increases and the depletion region becomes wider at the LSMO/BFO interface, accompanied with upward band bending and an enhanced Schottky barrier. Correspondingly, the built-in field decreases, and the depletion region becomes narrower at the Au/BFO interface, and the band bending goes down. Therefore, after upward polarization, the Schottky barriers at the LSMO/BFO interface dominate in the transport property, and the heterostructure works as a forward diode (as shown in Fig. 3(b)). On the other hand, for the Au/BFO/LSMO/STO heterostructure after downward polarization, the Schottky barrier at the Au/BFO interface dominates the transport property of the Au/BFO/LSMO/STO heterostructure, and the heterostructure works as a reverse diode (as shown in Fig. 3(b)). Therefore, the junction resistance after upward polarization (downward polarization) is at the low-resistance (high-resistance) state when the read voltage is −1 V, as shown in Fig. 2(a). With the polarization reversal, the direction of the built-in field in the Au/BFO/LSMO/STO heterostructure can be reversed. Therefore, the signs of I_{sc} and V_{oc} are opposite for two different polarization states

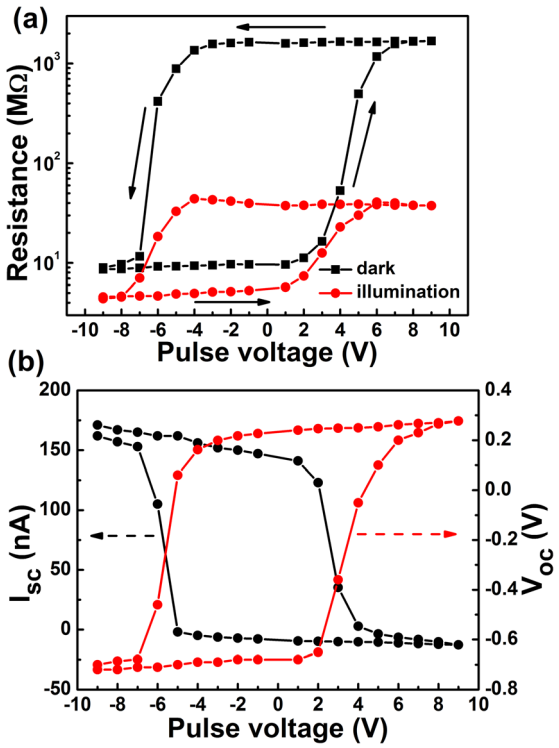

FIG. 4. (a) Bipolar resistance switching hysteresis loops for the Au/BFO/LSMO/STO heterostructure in dark and under the illumination of the 375 nm laser (840 mW/cm^2). The measurement voltage is −1 V. (b) I_{sc} and V_{oc} of the Au/BFO/LSMO/STO heterostructure with various pulse voltages under the illumination of the 375 nm laser (840 mW/cm^2), where each point represents the value summarized from the illuminated *I-V* curves.

in the Au/BFO/LSMO/STO heterostructure (as shown in Fig. 3(b)). The photo-induced electron-hole pairs can be generated and separated by the build-in field and the depolarization field, when the Au/BFO/LSMO/STO heterostructure is illuminated by the 375 nm laser with photon energy larger than the band-gaps of materials. Another two resistance states can be induced under the illumination of the 375 nm laser, as shown in Fig. 2(a). Therefore, four stable resistance states can be achieved. Moreover, the larger Schottky barrier at the Au/BFO interface will provide a higher built-in field as a driving force to separate the photo-generated electron-hole pairs more efficiently. Therefore, larger magnitudes of the V_{oc} and I_{sc} in the Au/BFO/LSMO/STO heterostructure after downward polarization are observed.

In order to investigate the ferroelectric evolution on the junction resistance and the switchable photoelectric effect, we measured the junction resistances and the *I-V* curves of the Au/BFO/LSMO/STO heterostructure in dark and under the illumination of the 375 nm laser at various pulse voltages. Figure 4(a) shows bipolar resistance switching hysteresis loops in dark and under the illumination of the 375 nm laser. The measurement voltage was −1 V. The resistance switching hysteresis loops are similar to the *P-E* loop as shown in Fig. 1(b). I_{sc} and V_{oc} of the Au/BFO/LSMO/STO heterostructure are also hysteretic as a function of pulse voltage, as shown in Fig. 4(b). These characteristics confirm that the ferroelectric polarization plays a very important role in the electro-resistance effect and the switchable photoelectric effect.

In summary, we report an electric-photo double modulation on the resistive switching behavior in the Au/BFO/LSMO/STO heterostructure. The high or low resistance states of the heterostructure can be switchable by applying pulse voltages with the opposite polarization directions, and the ratio of the high-low resistance states can be modulated by the laser illumination, which is due to the combination of electro-resistance and photo-resistance effects. The switchable photoelectric effect was also investigated. The directions of V_{oc} and I_{sc} are reversely switchable by applying electric voltage pulses, and the direction of I_{sc} is always opposite to the diode's forward direction. We proposed that the modulation of Schottky barriers, which are mainly related to the ferroelectric polarization, is responsible for the observed electro-resistance effect and switchable photoelectric effect. Our results will open a way for potential applications in combining multiple degrees of freedom in the resistance memory.

This work was supported by the National Basic Research Program of China (Nos. 2012CB921403 and 2013CB328706) and the National Natural Science Foundation of China (Nos. 11134012 and 11174355).

[1]W. Känzig, *Ferroelectrics and Antiferroelectrics in Solid State Physics* (Academic, New York, 1957), Vol. 4, pp. 5–6.
[2]V. Garcia, S. Fusil, K. Bouzehouane, S. Enouz-vedrenne, N. D. Mathur, A. Barthelemy, and M. Bibes, Nature **460**, 81 (2009).
[3]R. Ramesh and N. A. Spaldin, Nature Mater. **6**, 21 (2007).
[4]J. F. Scott, Nature Mater. **6**, 256 (2007).
[5]D. S. Rana, I. Kawayama, K. Mavani, K. Takahashi, H. Murakami, and M. Tonouchi, Adv. Mater. **21**, 2881 (2009).
[6]W. Ji, K. Yao, and Y. C. Liang, Adv. Mater. **22**, 1763 (2010).
[7]S. Y. Yang, J. Seidel, S. J. Byrnes, P. Shafer, C. H. Yang, M. D. Rossell, P. Yu, Y. H. Chu, J. F. Scott, J. W. Ager III, L. W. Martin, and R. Ramesh, Nat. Nanotechnol. **5**, 143 (2010).
[8]H. T. Yi, T. Choi, S. G. Choi, Y. S. Oh, and S.-W. Cheong, Adv. Mater. **23**, 3403 (2011).
[9]M. Alexe and D. Hesse, Nat. Commun. **2**, 256 (2011).
[10]J. Kreisel, M. Alexe, and P. A. Thomas, Nature Mater. **11**, 260 (2012).
[11]A. Q. Jiang, C. Wang, K. J. Jin, X. B. Liu, J. F. Scott, C. S. Hwang, T. A. Tang, H. B. Lu, and G. Z. Yang, Adv. Mater. **23**, 1277 (2011).
[12]C. Wang, K. J. Jin, Z. T. Xu, L. Wang, C. Ge, H. B. Lu, H. Z. Guo, M. He, and G. Z. Yang, Appl. Phys. Lett. **98**, 192901 (2011); C. Ge, K. J. Jin, C. Wang, H. B. Lu, C. Wang, and G. Z. Yang, J. Appl. Phys. **111**, 054104 (2012).
[13]L. Wang, Y. L. Jin, K. J. Jin, C. Wang, H. B. Lu, C. Wang, C. Ge, X. Y. Chen, E. J. Guo, and G. Z. Yang, Europhys. Lett. **96**, 17008 (2011).
[14]G. Z. Yang, H. B. Lu, Z. H. Chen, D. F. Cui, H. S. Wang, H. Q. Yang, F. Y. Miao, Y. L. Zhou, and L. Li, Sci. China, Ser. A: Math., Phys., Astron. **28**, 260 (1998); H. B. Lu, S. Y. Dai, Z. H. Chen, G. Z. Yang, Y. L. Zhou, M. He, L. F. Liu, H. Z. Guo, Y. Y. Fei, and W. F. Xiang, Appl. Phys. Lett. **86**, 032502 (2005); K. J. Jin, H. B. Lu, Q. L. Zhou, K. Zhao, B. L. Cheng, Z. H. Chen, Y. L. Zhou, and G. Z. Yang, Phys. Rev. B **71**, 184428 (2005).
[15]T. L. Qu, Y. G. Zhao, D. Xie, J. P. Shi, Q. P. Chen, and T. L. Ren, Appl. Phys. Lett. **98**, 173507 (2011).
[16]F. Yan, G. Chen, L. Lu, and J. E. Spanier, ACS Nano **6**, 2353 (2012).
[17]C. T. Nelson, P. Gao, J. R. Jokisaari, C. Heikes, C. Adamo, A. Melville, S. H. Baek, C. M. Folkman, B. Winchester, Y. J. Gu, Y. M. Liu, K. Zhang, E. G. Wang, J. Y. Li, L. Q. Chen, C. B. Eom, D. G. Schlom, and X. Q. Pan, Science **334**, 968 (2011).
[18]M. P. de Jong, V. A. Dediu, C. Taliani, and W. R. Salaneck, J. Appl. Phys. **94**, 7292 (2003).
[19]S. J. Clark and J. Robertson, Appl. Phys. Lett. **90**, 132903 (2007).
[20]R. R. Mehta, B. D. Silverman, and J. T. Jacobs, J. Appl. Phys. **44**, 3379 (1973).
[21]B. C. Huang, Y. T. Chen, Y. P. Chu, Y. C. Huang, J. C. Yang, Y. C. Chen, and Y. H. Chu, Appl. Phys. Lett. **100**, 122903 (2012).